R.Umamaheswara rao, S.Santhosh Kumar, M.Santhi Kumar / International Journal of Engineering Research and Applications (IJERA) ISSN: 2248-9622 www.ijera.com
Vol. 2, Issue4, July-August 2012, pp.1451-1458

Preparation And Characterization Of Polymer Nanocomposites For Damping.

R.Umamaheswara rao[1], S.Santhosh Kumar[2], M.Santhi Kumar[3].
(Department of Mechanical Engineering, GMR Institute of Technology, Rajam-532127.
Srikakulam District, Andhra Pradesh, INDIA.

ABSTRACT

Carbon nanotube-based composite is becoming increasingly popular and offers great potential for highly demanding practical high strength and high damping applications. The excellent damping capacity of CNTs is primarily due to the interfacial friction between carbon nanotubes and polymer resins and the extremely large interfacial surface area over a given specific mass (specific area). In this work pure MWCNT were used to blend with PLA and composite was prepared by melt-mixing under different CNT loadings. Especially we concentrated on Dynamic characterization of the nanocomposite. Dynamic characterization is done by using DMA in which loss modulus, storage modulus and damping loss factor variations were determined with respect to frequency. We interpreted DMA conditions in ANSYS and found amplitude which is input for theoretical model based on interfacial friction between the PLA and MWCNT. The model, developed is analytical and relates explicitly the material properties of the resin (PLA) and nanotubes and the processing parameters to the overall material damping loss factor and hence it offers the possibility for material engineers to possibly optimize the damping for required applications.

Keywords - vibration of nanotubes, vibration damping, damping of nanotubes, nanocomposite Damping of nanocomposite, vibration of nanocomposite

1. INTRODUCTION

With the advances in technology and the increase in the global population, plastic materials have found wide applications in every aspect of life and industries. However, most plastics such as polyethylene, polypropylene, and polystyrene are non biodegradable, and their increasing accumulation in the environment has been a threat to the planet. To overcome all these problems, some steps have been undertaken.PLA, though discovered, & Enhancement of damping in a structural system can lead to alleviation of aero elastic flutter, reduction of gust loading, increased fatigue life of structural components, improved cabin noise, maneuverability and handling. In fact, high structural damping is an Important design parameter for all machine elements and manufacturing tools. In addition, enhancement of damping holds the potential for improving Tracking and positioning characteristics such as those of a read/write head of a computer hard disk drive and the accuracy of the weapon systems mounted on aircrafts and land systems. Other applications of damping enhancement range from turbo-machinery and engine/equipment mounts to suspension and steering systems in automotive engineering. Therefore, it is necessary to develop structural components with high level of mechanical damping for a wide variety of applications in aerospace, mechanical and civil engineering systems. Viscoelastic materials such as high loss factor polymers have been the most frequently used in modern damping applications [1–5]. Elastomeric materials operated in simple shear were investigated both experimentally and analytically and were used for helicopter damper applications [6]. Performance characteristics of magnetic constrained layer damping had been investigated by Baz and Poh [7]. Vibration/shock absorbers were developed for automotive suspension applications using electro-rheological fluids by Lindler and Wereley [8]. On the other hand, damping properties of magneto-rheological fluids were investigated by Kamath et al. [9] and dampers for helicopter rotor blade applications were developed. Using a passive capacitive shunt circuit, tunable solid-state piezoelectric vibration absorbers have been investigated and developed for general aerospace applications [10]. Recent research effort in this direction has been much focused on the development of polymer damping materials based on nanocomposites in which nanotubes, nanofibers or nanoparticles are embedded in polymer substrates and much promising results have been established. Nanocomposites with embedded carbon nanotubes have recently been rigorously pursued for their superb mechanical strength as well as their potential damping capacities [11–13]. In addition, other types of nanocomposites have also been investigated such as those modified with nanoclay [14–15] and have been found effective for damping applications. This report, however, will focus on the modeling of damping mechanism of carbon nanotube-based nanocomposites. which is used for converting non linear spring characteristics to linear form. By conducting harmonic analysis in ANSYS we found the amplitudes for the testing specimen and these amplitudes were used as inputs for the mathematical model.

2. MELT BLENDING

2.1. Processing of PLA with MWCNT:

Prior to processing, PLA was dried in an oven set at 55ºC for four hours to remove any absorbed moisture.PLA is blended with MWCNT in the following four different proportions.

» PLA + 0.2 wt% MWCNT
» PLA + 0.5 wt% MWCNT
» PLA + 1.0 wt% MWCNT
» PLA + 2.0 wt% MWCNT

Finally, the PLA and MWCNT neat resin were extruded using a 32-mm (L/D = 20) Davis Standard co-rotating twin extruder at a temperature of 170ºC with 6 minutes duration at 50 rpm speed to create a polymer matrix of PLA and MWCNT of four different proportions mentioned above. The twin screw extruder was configured with mixing elements that were capable of providing additional shear. The extruded material then was chopped into small pellets using a pelletizer

2.2. COMPRESSION MOLDING:

Compression molding is a method of molding in which the molding material, generally preheated, is first placed in an open, heated mold cavity. The mold is closed with a top force or plug member, pressure is applied to force the material into contact with all mold areas, while heat and pressure are maintained until the molding material has cured. The process employs thermosetting resins in a partially cured stage, either in the form of granules, putty-like masses, or performs. Compression molding is a high-volume, high-pressure method suitable for molding complex, high-strength fiberglass reinforcements. Advanced composite thermoplastics can also be compression molded with unidirectional tapes, woven fabrics, randomly oriented fiber mat or chopped strand. The advantage of compression molding is its ability to mold large, fairly intricate parts.Also,it is one of the lowest cost molding methods compared with other methods such as transfer molding and injection molding; moreover it wastes relatively little material, giving it an advantage when working with expensive compound. However, compression molding often provides poor product consistency and difficulty in controlling flashing, and it is not suitable for some type of parts. Compression molding produces fewer knit lines and less fiber-length degradation than injection molding. According to ASTM D1238, specimen size of 25x6x4 mm was prepared by thread cutting

3. DMA (DYNAMIC MECHANICAL ANALYZER):

3.1. DMA-242Cspecifications

Temperature range=150-600degC
Frequency range=0.01-200Hz
Force range=0.0001-18N

3.2. PRINCIPLE OF DMA:

Dynamic mechanical analysis (DMA) yields information about the mechanical properties of a specimen placed in minor, usually sinusoidal, oscillation as a function of time and temperature by subjecting it to a small, usually sinusoidal, oscillating force. The applied mechanical load, that is, stress, elicits a corresponding strain (deformation) whose amplitude and phase shift can be determined.

3.3. TESTING MODE:

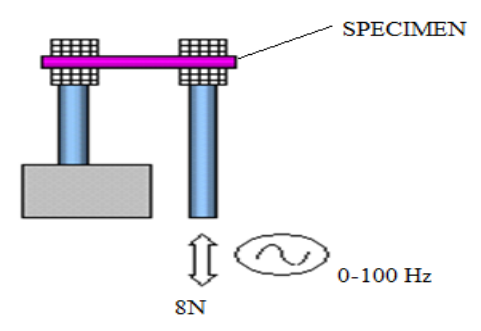

Figure 1: Single Cantilever mode

Specimen is clamped between the clamps as shown in above figure as one end is fixed and at the other end load is applied with a frequency range of 0-100 Hz

3.4. RESULTS FROM DMA:

3.4.1. STORAGE MODULUS:

The storage modulus E´ represents the stiffness of a viscoelastic material and is proportional to the energy stored during a loading cycle. It is roughly equal to the elastic modulus for a single, rapid stress at low load and reversible deformation

3.4.2. LOSS MODULUS:

The loss modulus E´´ is defined as being proportional to the energy dissipated during one loading cycle. It represents, for example, energy lost as heat, and is a measure of vibrational energy that has been converted during vibration and that cannot be recovered.

3.4.3. DAMPING LOSS FACTOR:

The loss factor tanδ is the ratio of loss modulus to storage modulus. It is a measure of the energy lost, expressed in terms of the recoverable energy, and represents mechanical damping or internal friction in a viscoelastic system. The loss factor tanδ is expressed as a dimensionless number. A high tanδ value is indicative of a material that has a high, nonelastic strain component, while a low value indicates one that is more elastic.

4. THEORETICAL MODELING

This mathematical modeling is based on the interfacial friction losses between the nanotubes,

nanotubes and resin in the composite. This friction losses occurs due to shearing action of one layer over another while we apply load due to its viscoelastic nature.

4.1. Mathematical modeling:

Damping is physically an average measure of the rate of energy dissipation of a system. What are the major energy dissipation mechanisms present in a nanocomposite system with CNTs as reinforcements under cyclic loading? Three major sources can be clearly identified and these are: (i) the inherent material damping of the base polymer, (ii) the frictional loss resulting from the slips between CNTs and polymer resins and (iii), the frictional loss from the slips between CNTs themselves. Inherent material damping is 24 well understood and here we focus ourselves on the understanding and modeling of the frictional losses between CNTs and polymer resins and between CNTs themselves. First, let us examine an ideal case where dispersed MWCNTs are uniformly distributed among resins and are all ideally oriented along the axial direction as shown in Fig.

Fig.2. Polymer with reinforced carbon nanotubes

From vibration analysis point of view, such a cell element can be modeled as a mass spring system with 3 springs representing the stiffness of the resin, the nano tube outer layer and the nano tube inner layer as shown in Fig.10. Here kR, k1 and k2 represent the stiffness and mR, m1 and m2 represent the masses of the resin, the outer layer of the carbon nanotubes and the inner layers of the carbon nanotubes respectively. Therefore f1 and f2 represent the interfacial friction limits between the resin and the nanotubes and between the nanotubes at which slips between the surfaces occur. These parameters of the model can be determined from the given material properties of the resin and the nanotubes such as Young's modulus and the processing parameters such as volume fraction.

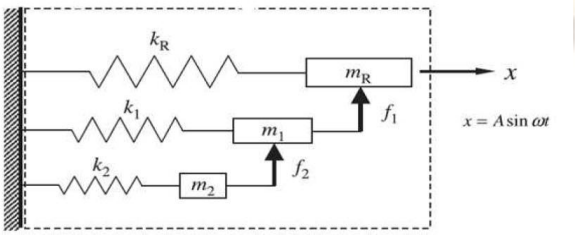

Fig.3.Vibration analysis model of the basic cell element

Volumefraction $\emptyset = \pi r^2 l/\pi R^2 l$ (1)

Stiffness of the resin $K_R = \pi E_R r^2/l\emptyset$ (2)

Stiffness of the outer layer $K_1 = E_n A_1/l$ (3)

Stiffness of the outer layer $K_2 = E_n A_2/l$ (4)

Where E_r and E_n are the Young's moduli of the resin and the nanotubes, respectively. Further assume the critical stresses between the resin and the nanotubes and between the nanotubes at which slips occur to be t1 and t2, and then interfacial friction limits can be written as

$f_1 = 2\pi r l \tau_1$ (5)

$f_2 = 2\pi r_1 l \tau_2$ (r_1 Is radius of the inner layer) (6)

The value of *l* can be selected as the typical length of the nanotube reinforcement. The inertial forces during vibration low frequencies can be neglected.

4.2. Vibration analysis:

Based on the basic cell element shown in Fig.10, one can derive its force-displacement relationships. Define $\delta_1=f_1/k_1$, $\delta_2=f_2/k_2$ and assume $\delta_1\leq\delta_2$, then when there is a displacement actuation input x=Asinwt, the force output of the element can be established for the for the following actuation amplitude A

4.2.1. Interfacial slips between resin and nanotubes and nanotubes themselves:

When the input actuation amplitude becomes large ($A\geq\delta_2$) both the interface between the resin and the nanotubes and that between the nanotubes themselves starts to slip and substantial friction loss will be generated leading to high level of mechanical damping capacity. The force-displacement relationship in this case can be shown in fig.

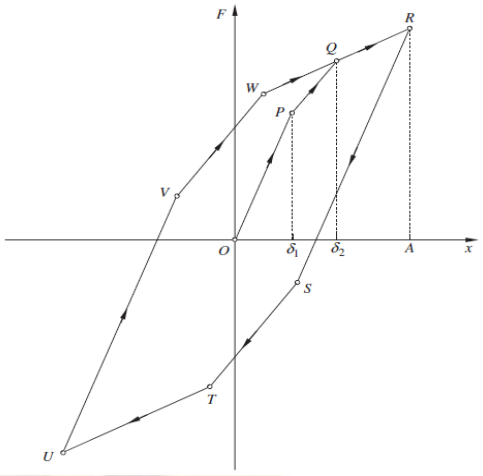

Fig.4. Force-Displacement relationship

It is first appropriate to examine this general case to see how a hysteretic loop is formed and hence energy dissipated during a vibration cycle. When x starts it increase but is less than δ1, the force-displacement relationship follows the line OP with an effective stiffness the sum of the three individual stiffness, $K=K_1+K_2+K_r$. Once it reaches P, k_1 starts to slip. And the effective stiffness becomes $K=K_r+K_2$ until it gets to Q at which K_2 also starts to slip. Hence from Q to R, the effective stiffness becomes $K=K_r$. It then follows RS on its way back with no slip and then ST with K_1 slipping and TU with both K_1 and K_2 is slipping at the same time. Finally, it follows UV, VW and WQ back to Q and a complete cycle under the

sinusoidal displacement actuation. Having now established the force-displacement relationship, from it one can derive the damping loss factor of the cell, which is also the damping loss factor of the nanocomposite material concerned. However, the simple fact that the force-displacement relationship involves a hysteretic loop implies that such a system model is nonlinear with memory and some appropriate linearization procedure is required before damping loss factor of the system can be established. The most powerful and frequently used method, which can be employed to derive an accurate equivalent linearized model for a nonlinear characteristics shown in above fig. Describing function is used here to linearize the non linear characteristics.

Sinusoidal input is

$$X = A\sin\omega t = A\sin\emptyset \quad (7)$$

A and w are constants and output can be expressed in Fourier expression is

$$f(X,\dot{X}) = f(A\sin\emptyset, A\omega\cos\emptyset) = \sum_{n=1}^{\infty}(a_n\sin n\emptyset + b_n\cos n$$

(8)

Where a_n and b_n (n=1, 2, 3---) are real constants to be determined. The first two fundamental terms can be derived by multiplying both sides by $sin\emptyset$ and $cos\emptyset$ integrating over [0,2π] with respect to $\emptyset$ as

$$a_1 = \int_0^{2\pi} f(A\sin\emptyset, A\omega\cos\emptyset)\sin\emptyset\, d\emptyset$$

(9)

$$b_1 = \frac{1}{\pi}\int_0^{2\pi} f(A\sin\emptyset, A\omega\cos\emptyset)\cos\emptyset\, d\emptyset$$

(10)

Here $a1 = a1$ (A, w) and b1=b1 (A, w), hence the output of first order approximation is

$$f(A\sin\emptyset, A\omega\cos\emptyset) = a_1\sin\emptyset + b_1\cos\emptyset$$

(11)

Using complex notation above equation can be written as

$$f(A\sin\emptyset, A\omega\cos\emptyset) = a_1\sin\emptyset + b_1\sin(\emptyset + (\pi/2))$$

$$= a_1\sin\emptyset + ib_1\sin\emptyset$$

(12)

Now we can define first order transfer function H1 (A, w) of the nonlinearity which is the ratio between output and the input

$$H_1(A,\omega) = (a_1\sin\emptyset + ib_1\sin\emptyset/A\sin\varphi)$$

$$= (a_1 + ib_1)/A$$

(13)

It should be noted that H1 (A, w) is the transfer function of the equivalent linearized system of the non linearity corresponding to that particular input amplitude A. Such transfer function is also defined as describing function N (A, w) under harmonic excitation.

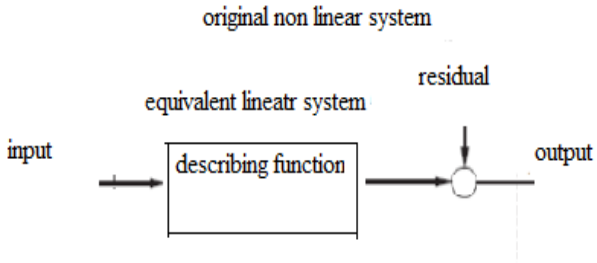

Fig.5. Describing Function

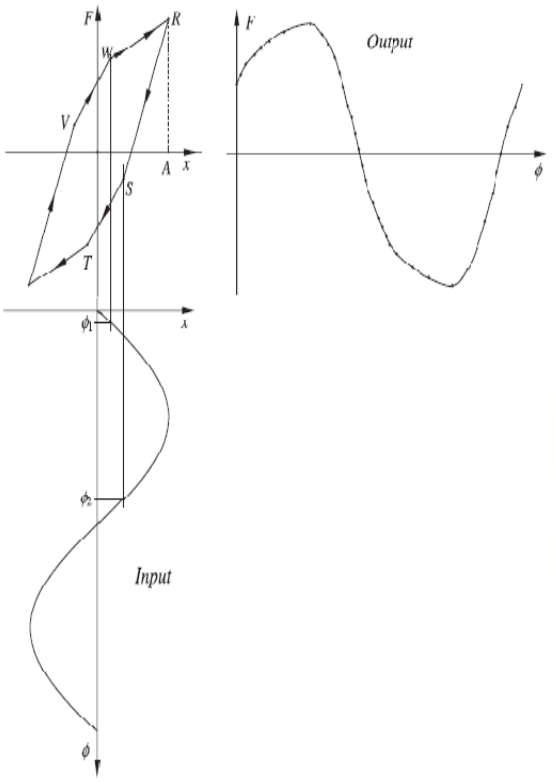

Fig.6. input-output characteristics of the non linear force-displacement relationship.

The sinusoidal input and the output of the nonlinearity can be sketched as shown in Fig.13. First, we need to establish the coordinates of points S and W and with little analysis of the hysteresis characteristics one can obtain,

S: $(A-2\delta_1, k_2\delta_2+k_rA-k_1\delta_1-2k_2\delta_1-2kr\delta_1)$

W: $(2\delta_2-A, k_1\delta_1+k_2\delta_2+2kr\delta_2-krA)$

From the above points we can get both $\emptyset 1$ and $\emptyset 2$. With these describing function can be written as

$$a1 = \frac{1}{\pi}\int_0^{2\pi} f(A\sin\emptyset, A\omega\cos\emptyset)\sin\emptyset\, d\emptyset = \frac{2}{\pi}\int_{\emptyset 1}^{\pi+\emptyset 1} f(A\sin\emptyset, A\omega\cos\emptyset)\sin\emptyset\, d\emptyset$$

(14)

$$= \frac{2}{\pi}\left(\int_{\emptyset 1}^{\frac{\pi}{2}} f(A\sin\emptyset, A\omega\cos\emptyset)\sin\emptyset\, d\emptyset + \int_{\frac{\pi}{2}}^{\emptyset 2} f(A\sin\emptyset, A\omega\cos\emptyset)\sin\emptyset\, d\emptyset + \int_{\emptyset 2}^{\pi+\emptyset 1} f(A\sin\emptyset, A\omega\cos\emptyset)\sin\emptyset\, d\emptyset\right) \quad (15)$$

$$b1 = \frac{1}{\pi}\int_{0}^{2\pi} f(A\sin\emptyset, A\omega\cos\emptyset)\cos\emptyset\, d\emptyset = \frac{2}{\pi}\int_{\emptyset 1}^{\pi+\emptyset 1} f(A\sin\emptyset, A\omega\cos\emptyset)\cos\emptyset \quad (16)$$

WR: $F=Kr*x+K_1*\delta_1+K_2*\delta_2$
RS: $F= (Kr+K_1+K_2)*x+K_1*\delta_1+K_2*\delta_2-K_1*A-K_2*A$
ST: $F= (Kr+K_2)*x+K_2*\delta_2-K_2*A- K_1*\delta_1$
From this we can find out the damping loss factor as

$$\eta = \frac{b1}{a1} \quad (17)$$

5. RESULTS AND DISCUSSIONS

5.1. EXPERIMENTAL RESULTS

5.1.1. STORAGE MODULUS VARIATION WITH FREQUENCY

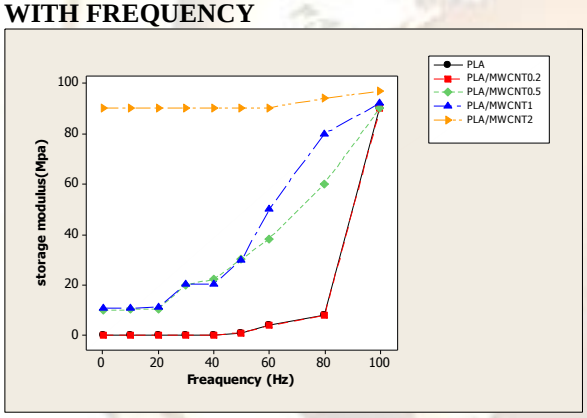

Fig.7.Frequency Vs Storage modulus

The dynamic storage moduli obtained from the dynamic frequency sweep are shown in Figure 7. The shoulder presented on the modulus curve of the blank PLA sample (see the arrow in Figure 7) is attributed to the shape relaxation. During oscillatory shear flow, the total area of the interface as well as the interfacial energy is changing periodically but with a much longer relaxation time than that of component polymers. This kind of long relaxation due to the presence of interface leads to an additional transition shoulder on the modulus curves. It is seen that the relaxation shoulder shifts to low-frequency region with small addition of the MWCNTs (0.2 phr).

5.1.2. LOSS MODULUS VARIATION WITH FREQUENCY

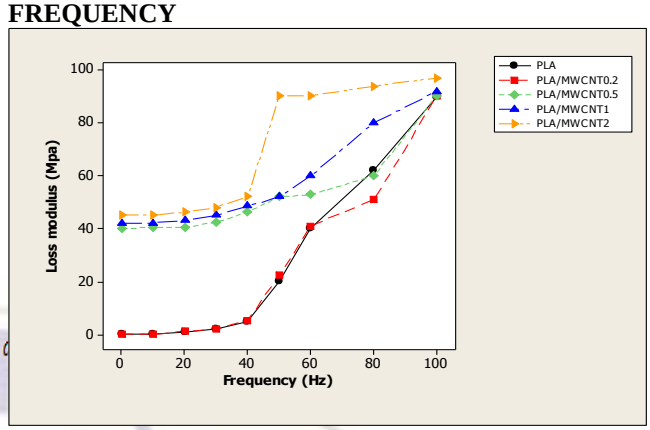

Fig.8.Frequency Vs Loss modulus

The loss module obtained from the dynamic frequency sweep is shown in Figure 8. During oscillatory shear flow, the total area of the interface as well as the interfacial energy is changing periodically but with a much longer relaxation time than that of component polymers. It is seen that the relaxation shoulder shifts to low-frequency region with small addition of the MWCNTs (0.2 phr). This indicates that the presence of MWCNTs retards shape relaxation of the PLA matrix .Because the interfacial relaxation time is proportional to the ratio between droplet size and the interfacial tension, longer interfacial relaxation process but with decreasing droplet size means a large decrease of interfacial tension. PLA sample and the frequency dependence nearly disappear. This conterminal behavior is due to formation of MWCNTs network, which highly restrains the long-range relaxation of the matrix.

5.1.3. DAMPING LOSS FACTOR VARIATION WITH FREQUENCY

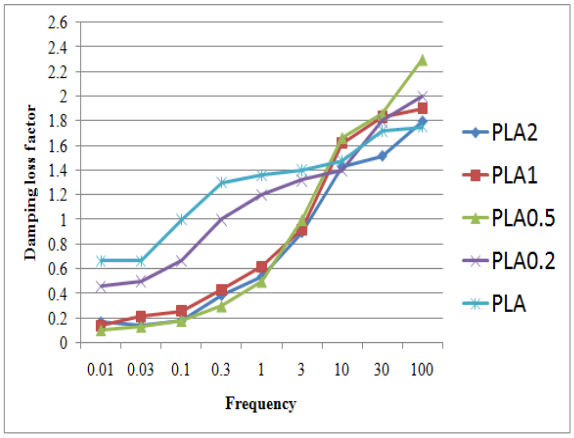

Fig.9. Frequency Vs Damping loss factor

The above graph shows damping loss factor for different nano composites. By increasing

MWCNT loadings in the matrix PLA up to addition of small amounts 0.2and 0.5 wt%. Further increase in MWCNT loadings such as 1 wt% and 2 wt% there is

decreased trend observed but these are having high damping loss factor than matrix PLA.

5.1.4. VALIDATION FOR PLA/MWCNT2% SAMPLE

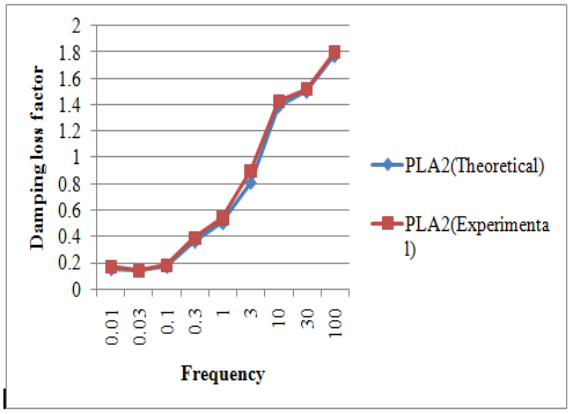

Fig.10.Variation of theoretical and experimental loss factor for PLA/MWCNT2% sample

The above graph shows the variation of theoretical damping loss factor from the experimental damping loss factor for the sample PLA/MWCNT2. Here the Damping loss factor is increasing when the frequency is increased.

Table.1.Validation of Theoretical with experimental results for PLA/MWCNT2%

PLA/MWCNT2 (Theoretical)	PLAMWCNT2 (Experimental)	% error
0.154	0.17	9.4
0.1428	0.14	1.9
0.1702	0.18	5.44
0.1362	0.39	10.43
0.502	0.54	5.66
0.81	0.9	10.88
1.39	1.43	8.53
1.5	1.52	6.88
1.77	1.8	5.38

5.1.5. VALIDATION FOR PLA/MWCNT1% SAMPLE

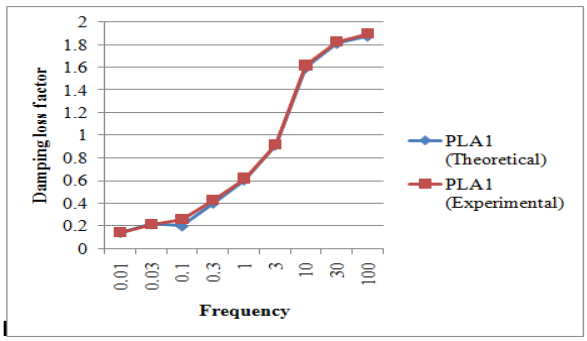

Fig.11.variation of theoretical and experimental loss factor for PLA/MWCNT1% sample.

The above graph shows the variation of theoretical damping loss factor from the experimental damping loss factor for the sample PLA/MWCNT1. And the damping loss factor is increasing when the frequency is increased in theoretically and experimentally.

In this graph there is almost a zero variation we can observed and theoretical model is more accurate in PLA/MWCNT1 than PLAMWCNT2.

Table .2. Validation of Theoretical with experimental results for PLA/MWCNT1%

PLA/MWCNT1 (Theoretical)	PLA/MWCNT1 (Experimental)	% error
0.139	0.142	2.1
0.215	0.214	0
0.197	0.26	0
0.399	0.43	1.4
0.6031	0.62	0
0.9105	0.92	10.67
1.595	1.62	5.4
1.81	1.83	3.6
1.875	1.9	2.2

5.1.6. VALIDATION FOR PLA/MWCNT0.5% SAMPLE

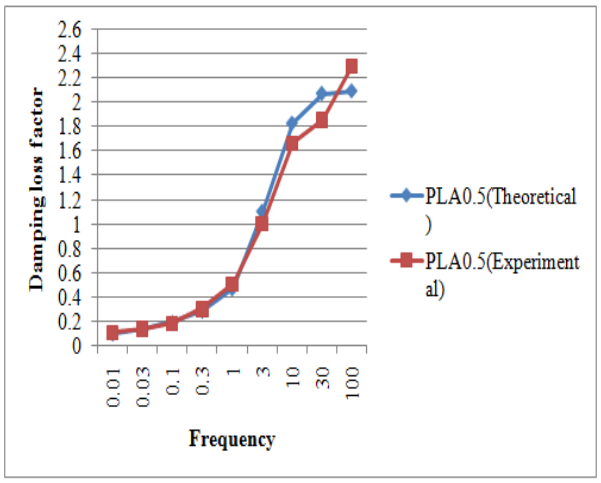

Fig.12.variation of theoretical and experimental loss factor for PLA/MWCNT0.5% sample.

The above graph shows the variation of theoretical damping loss factor from the experimental damping loss factor for the sample PLA/MWCNT0.5. And the damping loss factor is increased while increasing the frequency.

In this graph there is almost a zero variation we can observe and theoretical model is more accurate in PLA/MWCNT0.5 than both PLAMWCNT1 and PLA/MWCNT2.

Table 3: Validation of Theoretical with experimental results for PLA/MWCNT0.5%

PLAMWCNT0.5 (Theoretical)	PLAMWCNT0.5 (Experimental)	% error
0.09873	0.1066	7.3
0.1357	0.1357	0
0.1926	0.18	6.5
0.2852	0.3	4.93
0.4694	0.5	6.12
1.1061	1	9.59
1.831	1.667	9.33
2.0752	1.857	8.4
2.0962	2.3	4.58

5.1.7. VALIDATION FOR PLAMWCNT0.2% SAMPLE

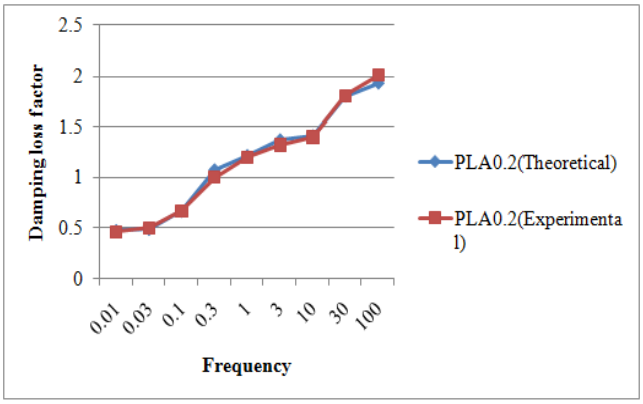

Figure13. Variation of theoretical and experimental loss factor for PLA/MWCNT0.2% sample

The above graph shows the variation of theoretical damping loss factor from the experimental damping loss factor for the sample PLA/MWCNT0.2%. The theoretical values for this sample found by using amplitudes obtained from ANSYS for the proposed interfacial friction model. These theoretical values mainly dependent on amplitude of the specimen.
In this graph there is almost a zero variation we can observe and theoretical model is more accurate in PLA0.2 than the other samples which are PLA2, PLA1 and PLA0.5.

Table 4: Validation of Theoretical with experimental results for PLA0.2

PLA/MWCNT0.2 (Theoretical)	PLA/MWCNT0.2 (Experimental)	% error
0.472	0.458	2.96
0.483	0.5	5.86
0.662	0.667	0
1.073	1	9.2
1.214	1.2	3.54
1.37	1.32	2.1
1.409	1.4	8.73
1.802	1.8	9.2
1.93	2	7.05

6. CONCLUSIONS

From experimental results, damping loss factor increases by increasing CNT loadings up to 0.5 wt% loading of MWCNT and thereby loss factor decreases by increasing the loading of MWCNT.
And also Proposed mathematical model is validated by experimental results and the maximum

deviation observed from the experimental results to the theoretical results.

With minimum error this proposed mathematical model can be used for the extrapolation for different nanocomposites.

References

[1] J.M.Biggerstaff, J.B.Kosmatka, *Damping performance of co cured graphite/epoxy composite laminates with embedded damping materials,* J.Compos. Mater. *33*(1999)1457–1469.

[2] J.B.Kosmatka, S.L.Liguore, *Review of methods for analyzing constrained layer damping structures*, J.Aerosp.Eng.*6* (1993)268–283.

[3] A.Baz, J.Ro, *The concept and performance of active constrained layer damping treatments*, J.SoundVib.*28* (1994)18–21.

[4] W.H.Liao, K.W.Wang, On *the analysis of viscoelastic materials for active constrained layer damping treatments*, J.SoundVib.*207* (1997)319–334.

[5] Y.Liu, K.W.Wang, *Anon dimensional parametric study of enhanced active constrained layer damping treatments*, J.SoundVib.*223* (1999)611–644.

[6] C.R.Brackbill, G.A.Lesieutre, E.C.Smith, L.E.Ruhl, *Characterization and modeling of the low strain amplitude and frequency dependent behavior of elastomeric damper materials,* J.Am.HelicopterSoc.*45* (1) (2000)34–42.

[7] A.Baz, S.Poh, *Performance characteristics of the magnetic constrained layer damping*, ShockVib.*7* (2) (2000)81–90.

[8] J.E.Lindler, N.M.Wereley, *Double adjustable shockabsorbersusing electro rheological fluid*, J.Intell.Mater.Syst.Struct.*10* (8) (1999)652–657.

[9] G.M.Kamath, N.M.Wereley, M.R.Jolly, *Characterization of magneto rheological helicopter lag dampers*, J.Am.HelicopterSoc.*44* (3) (1999)234–248.

[10] C.L.Davis, G.Lesieutre, *An active lytuned solid state vibration absorber using capacitive shunting of piezoelectric stiffness*, J.SoundVib. *232*(3) (2000) 601–617.

[11] N.Koratkar, B.Wei, P.M.Ajayan, *Carbonnanotube films for damping applications, Advanced Materials*, vol.*14*, pp.997–1000, 2002.

[12] X.Zhou, E.Shin, K.W.Wang, C.E.Bakis, *Interfacial damping characteristics of carbonnanotube-based composites*, Compos.Sci.Technol.*64* (2004) 2425–2437.

[13] J.Suhr, N.Koratkar, P.Keblinski, P.Ajayan, *Viscoelasticity in carbon nanotube composites*, Nat.Mater. *4*(2005)134–137.

[14] H.T.Chiu, J.H.Wu, Z.J.Shong, *Dynamic properties of rubber vibration is olatorsandanti vibration performance of nanoclay-modified PU/PEL blends system*, Polym.Eng.Sci. (2005)539–548.

[15] R.A.Kalgaonkar,J.P.Jog,*Copolyester/layered silicate nanocomposites: the effect of molecular size and structure of the intercalantonthe structure and viscoelastic properties of nanocomposites*, J.Polym.Sci: PartB: Polym.Phys.*41* (2003)3102–3113.